Journal of Rock Mechanics and Geotechnical Engineering 11 (2019) 46–60

Contents lists available at ScienceDirect

Journal of Rock Mechanics and Geotechnical Engineering

journal homepage: www.rockgeotech.org

Full Length Article

Numerical analyses of pillar behavior with variation in yield criterion, dilatancy, rock heterogeneity and length to width ratio

Sankhaneel Sinha*, Gabriel Walton

Colorado School of Mines, Golden, CO, USA

ARTICLE INFO

Article history:
Received 2 April 2018
Received in revised form
6 June 2018
Accepted 9 July 2018
Available online 22 September 2018

Keywords:
Rock pillars
Progressive S-shaped criterion
Numerical modeling

ABSTRACT

With recent advances in numerical modeling, design of underground structures increasingly relies on numerical modeling-based analysis approaches. While modeling tools like the discrete element method (DEM) and the combined finite-discrete element method (FDEM) are useful for investigating small-scale damage processes, continuum models remain the primary practical tool for most field-scale problems. The results obtained from such models are significantly dependent on the selection of an appropriate yield criterion and dilation angle. Towards improving its capabilities in handling mining-related problems, the authors have previously developed a new yield criterion (called progressive S-shaped criterion). The focus of the current study is to demonstrate its use in modeling rock pillars through a comparative analysis against four other yield criteria. In addition to the progressive S-shaped criterion, only one out of the four other criteria predicted a trend in strength consistent with an empirical pillar strength database compiled from the literature. Given the closely-knit relationship between yield criteria and dilation angle in controlling the overall damage process, a separate comparison was conducted using a mobilized dilation model, a zero degree dilation angle and a constant non-zero dilation angle. This study also investigates the impact of meso-scale heterogeneity in mechanical properties on the overall model response by assigning probability distributions to the input parameters. The comparisons revealed that an isotropic model using a combination of progressive S-shaped criterion and mobilized dilation angle model is sufficient in capturing the behaviors of rock pillars. Subsequently, the pillar model was used to assess the effect of L/W (length/width) ratio on the peak strength.

1. Introduction

Over the last decade, significant advances have been made in numerical modeling tools in terms of their ability to simulate physical phenomena at a wide range of scales as well as the associated computational capabilities. In the field of rock mechanics, large-scale design problems are often geometrically complex and are further exacerbated by the heterogeneous nature of most rock masses. Although empirical relationships can provide rough design parameters, they are generally constrained by limitations of the database which was used for their development. Furthermore, field-scale testing programs developed to minimize the need for abstract analyses may be infeasible due to the associated costs. Numerical modeling tools represent a convenient alternative for the purposes of analysis and design. While the discrete element method (DEM) and the finite-discrete element method (FDEM) are better suited for investigating small-scale rock damage processes (Munjiza, 2004; Jing and Stephansson, 2007; Ghazvinian et al., 2014; Lisjak and Grasselli, 2014; Farahmand and Diederichs, 2015; Yan et al., 2016; Mayer and Stead, 2017), continuum approaches remain the primary practical tool for mine-scale simulations. The outputs obtained from these models are significantly dependent on the choice of a yield criterion (Hajiabdolmajid et al., 2002; Edelbro, 2010; Walton et al., 2015).

Recently, the authors have developed a rock yield criterion that accounts for different failure modes of sparsely fractured rock masses over a wide range of expected confining stresses. In order to highlight the relative advantages of using this criterion, a comparative analysis has been performed in this study with four other yield criteria being considered. An associated goal is also to investigate the effect of meso-scale heterogeneity on the overall behavior of these models, as it has not been widely studied in the

* Corresponding author.
E-mail address: sankhaneelsinha@mymail.mines.edu (S. Sinha).

Peer review under responsibility of Institute of Rock and Soil Mechanics, Chinese Academy of Sciences.

https://doi.org/10.1016/j.jrmge.2018.07.003

literature. Because mine pillars are well-studied structures in the field of rock mechanics, they have been chosen as the primary context for this study.

A pillar typically fails through tensile fracturing in the outer peripheral region and through shearing in the inner confined portions. Previous studies have found conventional shear yield criteria to be inadequate in capturing the brittle spalling process (Pelli et al., 1991; Martin, 1997). As a result, the cohesion-weakening-frictional-strengthening (CWFS) strength model was formulated. Over the years, this strength model has been successfully used in modeling brittle damage near underground excavations (Hajiabdolmajid et al., 2002; Edelbro, 2009; Walton et al., 2016; Renani and Martin, 2018). However, for modeling pillars, an integration of CWFS and shear yield is necessary because neither of the two criteria is capable of capturing the macroscopic pillar behavior on its own. To that end, the progressive S-shaped criterion was developed to account for both failure mechanisms.

A number of other yield criteria have been utilized in the past for modeling rock pillars. Some of the major yield criteria used for this purposes include the ultimate S-shaped criterion (Kaiser et al., 2011; Kaiser and Kim, 2015), strain-softening Mohr-Coulomb (MC) (Iannacchione, 1999; Mortazavi et al., 2009), brittle Hoek–Brown (HB) (Martin and Maybee, 2000) and CWFS strength model (Hajiabdolmajid et al., 2002; Walton et al., 2015). In order to avoid any confusion with the progressive S-shaped criterion, the non-progressive S-shaped criterion developed by Kaiser et al. (2011) will be termed as the ultimate S-shaped criterion in this paper. None of these studies demonstrated the ability of a continuum model to reproduce the empirically observed trend of pillar strength as a function of width to height ratio (W/H). This is unsurprising given that these modeling approaches do not properly account for the fundamental aspects of brittle rock behavior. The ability of the progressive S-shaped criterion to capture this trend is a direct consequence of its development based on the fundamental progressive damage mechanisms of intact rock (Sinha and Walton, 2017, 2018). In this study, a numerical comparison in FLAC^{3D} is used to identify the key differences between these various yield criteria.

Selection of a dilation model is equally important as the selection of an appropriate yield criterion. In the past, rock dilatancy has often been neglected by selecting zero dilation angles in numerical models (e.g. Edelbro, 2009; Chugh and Abbasi, 2012). Although this may be acceptable under certain geologic conditions, it is erroneous to extend it to hard rock pillars where excavation boundary dilatancy controls the failure dynamics (Walton et al., 2015). Laboratory tests have found that dilation angle varies as a function of plastic shear strain and confining stress, which can be adequately captured by a mathematical model (Alejano and Alonso, 2005; Zhao and Cai, 2010; Walton and Diederichs, 2015a). This study uses one such dilation model, called the Walton-Diederichs (WD) model (Walton and Diederichs, 2015a), in conjunction with the progressive S-shaped criterion to simulate rock pillar behavior. Since the dilation angle interacts with the yield criterion to ultimately control the overall model behavior, the models were re-run with zero and constant non-zero dilation angles and the responses were compared to that obtained using the WD model. This approach not only helped in isolating their influences but also highlighted the impact of using simplified representations of rock dilatancy on rock pillar behavior.

With respect to the issue of accounting for rock mass variability in numerical models, the overall rock mass is typically approximated by an equivalent homogenous medium in continuum models. While this approach has been successfully used in replicating in situ behavior (Walton et al., 2015; Sinha and Chugh, 2016), it is of interest to evaluate to what extent the stochastic consideration of variability in strength properties influences the overall model results. The effect of spatial variability in material has been previously investigated for slopes (Esterhuizen, 1990; Hsu and Nelson, 2006) and room and pillar mine panels (Reinsalu, 2000). In this study, based on the findings of Langford and Diederichs (2015), the input parameters of the progressive S-shaped criterion were randomly derived from a normal distribution with 5% and 10% coefficient of variation (CV) and assigned to individual elements in the model. The variability in the element-level properties was then correlated with the variability in the macro-behaviors of slender and squat pillars.

The previous comparative analyses led to the conclusion that a homogenized continuum model using progressive S-shaped yield criterion and a mobilized dilation model is sufficient in modeling rock pillars. Since the validity of the pillar model has been established through a comparison against an empirical pillar database (Sinha and Walton, 2018), it was utilized here to investigate the effect of L/W ratio on the pillar's strengths.

2. Progressive S-shaped criterion: Background and pillar modeling

Development of the progressive S-shaped criterion was prompted due to the inability of previous yield criteria to capture the expected behavior of rock pillars. The new criterion is based on the precursory works of Diederichs (2005), Kaiser et al. (2011) and Kaiser and Kim (2015) with modifications to account for the progressive nature of the micro-damage processes in rock. The cumulative plastic shear strain parameter (ε^{ps}) is well established as a proxy for brittle damage in continuum models and was utilized in the formulation of the progressive S-shaped criterion (Hajiabdolmajid et al., 2002; Zhao et al., 2010; Walton et al., 2015; Itasca, 2016). The criterion combines the CWFS strength model at low confinement and a shear yield model at higher confinement with an ultimate upper envelope conforming to S-shape, as proposed by Diederichs (2005). Fig. 1 shows a schematic illustration of the progressive S-shaped criterion. The approach in its current form is restricted to nearly-intact rock masses where the behavior is not significantly influenced by pre-existing fractures.

The criterion consists of three envelopes: (1) yield, (2) peak, and (3) residual; these three envelopes evolve into each other as a function of ε^{ps}. The blue line in Fig. 1 separates the low confinement (corresponding to CWFS model) and high confinement (corresponding to the shear yield) portions of the progressive S-shaped criterion while the red lines correspond to the intermediate envelopes. Mechanistically, the three envelopes are related to the damage thresholds in rocks and are briefly described as follows:

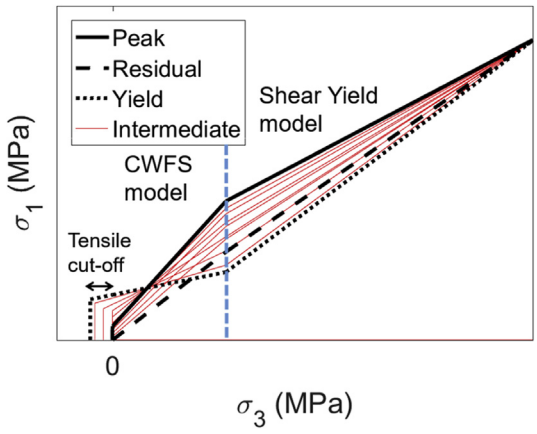

Fig. 1. Conceptual layout of the progressive S-shaped criterion (after Sinha and Walton, 2018).

(a) Yield envelope. The left portion corresponds to crack initiation (CI) threshold while the right portion is a modified form of the Mogi's line. This envelope marks the first point of yield in situ stress.
(b) Peak envelope. The yield envelope evolves to the peak envelope over a user-defined value of cumulative plastic shear strain. The left segment is related to the spalling limit while the right side corresponds to the crack damage (CD) threshold.
(c) Residual envelope. The peak envelope is degraded to the residual envelope over the entire range of expected confining stresses. The CI and CD thresholds can be estimated from laboratory test on intact rocks (Diederichs, 2005; Diederichs and Martin, 2010) while the spalling limit can be determined from the empirical relationship proposed by Diederichs (2005). Although the degradation of the peak to the residual envelope was based on the findings of Martin and Chandler (1994), this portion of the progressive S-shaped criterion is associated with some uncertainty and may require calibration when applied to specific case studies.

Justifications for the selection of these damage thresholds as part of the progressive S-shaped criterion and guidelines for determining the input parameters were provided by Sinha and Walton (2018). In this study, the parameters are chosen to conform to Creighton granite (uniaxial compressive stress, UCS $\approx$ 220 MPa), with values obtained from Sinha and Walton (2018). All simulations were run using the WD mobilized dilation angle model (Walton and Diederichs, 2015a). Tables 1 and 2 list the progressive S-shaped yield criterion and the WD model input parameters, respectively. When incorporated in a pillar model in FLAC^{3D} (Sinha and Walton, 2018), this type of model has been shown to replicate the hourglassing phenomenon (Krauland and Soder, 1987) and progressive localization of stress along the mid-height of the pillar (Wagner, 1974) observed in the field. To further test the reliability of the model results, the strength for different W/H ratios was overlaid on an empirical pillar strength database compiled from the literature. The database only considered cases studies with a rock UCS exceeding 200 MPa (comparable to the UCS of Creighton granite), and this resulted in inclusion of the datasets presented by Hedley and Grant (1972), Hudyma (1988) and Sjoberg (1992). It was found that the model results could precisely demarcate between the failed and stable case histories and exhibited a convex shape that is consistent with what has been typically associated with this relationship. The reader is referred to Sinha and Walton (2018) for additional details on this study.

3. Comparison with traditional continuum modeling approaches

With the ability of the progressive S-shaped criterion to replicate rock pillar behavior established by Sinha and Walton (2018), four other yield criteria, e.g. ultimate S-shaped (non-progressive), strain-softening MC, brittle HB, and CWFS strength criteria were chosen for the purpose of comparative analysis. To ensure that the models are comparable, the yield envelope in each case was developed using the most directly related segments of the progressive S-shaped criterion. The geometry of the pillar models is similar to that in Sinha and Walton (2018) with a mesh size of 0.166 m. The mesh size was selected based on a sensitivity analysis of its effect on the pre- and post-peak portions of the stress–strain responses.

Fig. 2a shows the brittle HB, strain-softening MC and CWFS envelopes while Fig. 2b illustrates the ultimate S-shaped envelope. All simulations employed the WD dilation angle model with parameters listed in Table 2 to isolate the influence of the strength model used on the results obtained.

For the strain-softening MC criterion, the peak and residual envelopes were chosen to correspond to the left side of the peak and residual envelopes of the progressive S-shaped criterion, respectively. The selection was based on the fact that the MC criterion was originally developed considering shear-based failures. In case of the brittle HB criterion, only one envelope was defined, following the suggestions of Martin and Maybee (2000). For the CWFS criterion, the peak and residual envelopes corresponded to the left side of the yield and peak envelopes of the progressive S-shaped criterion, respectively. In case of the ultimate S-shaped criterion, the peak envelope in regions (i) and (ii) (see Fig. 2b) was chosen to correspond to the yield and peak envelopes of the progressive S-shaped criterion, respectively. The residual envelope was derived by degrading the peak envelope and is described in further details in Section 3.1.

3.1. Ultimate S-shaped failure criterion

The need for a tri-linear or S-shaped failure criterion to reproduce hard rock behavior was first proposed by Diederichs (2005). Following his theoretical model, Kaiser et al. (2011) suggested the concept of confinement-dependent GSI (geological strength index) to capture the S-shaped criterion. The development of this approach was fueled by the flawed applicability of the generalized HB criterion in estimation of the confined rock mass strength (Valley et al., 2011; Bahrani et al., 2014). The S-shaped criterion considers tensile fracturing/spalling at low confinement and extensile-driven shear at high confinement (Diederichs, 2003), thereby providing realistic strength estimates for confined rock mass. The two segments of the criterion are connected by a transition zone where $\sigma_3/UCS = 1/10$. In the context of pillars, this means that elements having a confinement higher than $\sigma_3/UCS = 1/10$ (termed as outer shell) will fail through shearing while those below the threshold (termed as inner shell) will be subjected to spalling (Valley et al., 2011). The point of transition chosen, however, is speculative in nature. If this criterion is indeed used for modeling pillars, the threshold of transition should be modified preferably through a process of back-analysis.

Table 1
Thresholds and rock mass parameters relevant to the pillar model (Sinha and Walton, 2018).

Segments of the S-shaped envelope	Threshold in σ_1–σ_3 space (MPa)	Model input parameters		Plastic shear strain (10^{-3})
		Cohesion (MPa)	Friction angle (°)	
Yield (left portion)	$\sigma_1-\sigma_3 = 81$	40.5	0	0
Yield (right portion)	$\sigma_1-3.8\sigma_3 = -31.2$	−8	35.7	
Peak (left portion)	$\sigma_1-5.6\sigma_3 = 24.7$	5.3	44	10
Peak (right portion)	$\sigma_1-2.7\sigma_3 = 140.8$	43.2	26.9	
Residual (left potion)	$\sigma_1-3.9\sigma_3 = 0.4$	0.1	36.3	50
Residual (right portion)	$\sigma_1-3.5\sigma_3 = 17.5$	4.7	33.6	

Table 2
Rock mass dilation parameters used in model (Walton et al., 2015).

Pre-mobilization parameter (α_0)	Pre-mobilization confinement dependence (α')	Dilation mobilization plastic shear strain ($\epsilon^{PS}{}_m$)	Low confinement peak dilation parameter (β_0)	High confinement peak dilation parameter (β')	Dilation decay plastic shear strain parameter (ϵ^{ps*})
0.001	0.0038	0.0015	1.1	0.14	0.01

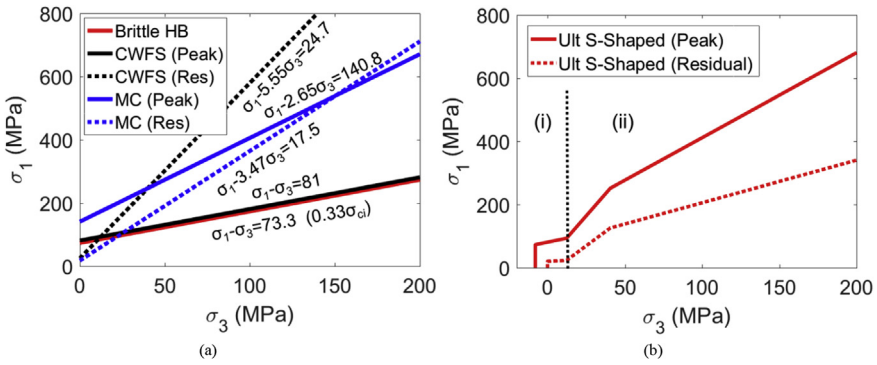

Fig. 2. Mathematical representation of the four different modeling techniques. In (b), the regions (i) and (ii) indicate where the yield and peak envelopes of the progressive S-shaped criterion are coincident with the peak envelope of the ultimate S-shaped criterion. σ_{ci} is the uniaxial compressive strength of the studied rock.

Using Rocscience software Phase^{2D}, Kaiser et al. (2011) assessed the effect of W/H on the strength of pillars. While it may not be possible to explicitly simulate pseudo-shearing associated with extensile crack localization in homogeneous continuum models, the overall damage evolution and change in mechanisms as a function of confinement at the meso-scale are represented by the S-shaped criterion. The model predicted an exponential increase in strength with W/H.

Although this approach has a strong theoretical basis, by only defining the ultimate strength envelope, it neglects the gradual localization of damage that occurs during loading. Thus it fails to account for the manner in which damage initiation and propagation can lead to unrealistic results. In Fig. 2b, the upper final envelope of the progressive S-shaped criterion was selected as the peak envelope for the ultimate S-shaped criterion, and a residual envelope was computed by lowering the higher and lower confinement peak strengths by 50% and 75%, respectively. Beyond the low confinement region ($\sigma_3 > 12.6$ MPa), yield occurs at the peak envelope. This is in direct contradiction with the findings of Walton et al. (2017) where yield in Indiana limestone samples initiated well below the peak strength under high confinement conditions. The use of only an ultimate envelope for modeling hard rocks essentially neglects the damage associated with CI and CD stress thresholds. Furthermore, the non-simultaneous mobilization of friction and cohesion for spalling-type failure is not considered in the manner that the residual envelope has been defined.

Six models corresponding to W/H ratios of 0.5, 1, 1.5, 2, 3 and 4 were run with peak to residual strength reduction over plastic shear strain of 0.04. The selection of an elastic-brittle-plastic constitutive model in Kaiser et al. (2011) may have been constrained by the available choices in Phase^{2D} - such is not the case in FLAC^{3D}. Also, modeling a strain-dependent degradation is necessary for comparison against the progressive S-shaped criterion. The ultimate S-shaped criterion was incorporated in FLAC^{3D} using the strain-softening MC constitutive model. A piece-wise FISH function was called every 1000 solution steps which modified the friction and cohesion of model elements as a function of confinement and plastic shear strain. The stress–strain curves for W/H ratios of 1, 2, 3 and 4 are shown in Fig. 3.

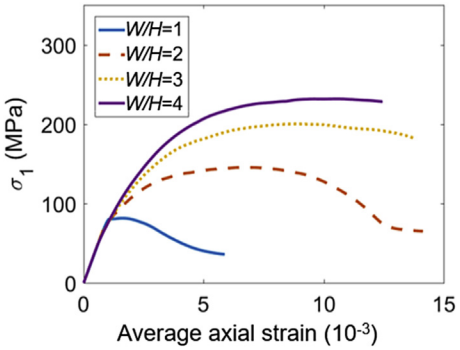

Fig. 3. Average stress–strain curves with $W/H = 1, 2, 3$ and 4 for the ultimate S-shaped criterion models.

Fig. 4 shows the strength curves for the progressive S-shaped criterion and the four modeling techniques tested. The peak strength for strain-hardening stress–strain curves (related to higher W/H models) was chosen as the point where the curve achieved its maximum. Here, only the strength curve corresponding to the ultimate S-shaped criterion will be discussed while the others will be discussed in their respective sub-sections. For lower ($\leq$1) and higher ($\geq$3) W/H ratios, the trend is similar to the progressive S-shaped criterion with a slightly higher overall strength. The major disparity in the shape of the curves occurs in W/H ratios of 1–3. This is likely due to the inability of the ultimate S-shaped criterion to account for the initial damage process that is associated with the CI stress threshold. It has been shown in Sinha and Walton (2018) that the peak strength of squatter pillars is controlled by the right side of the peak envelope. Given the identical envelopes in this region (see Fig. 2b), the two strength curves are expected to come close/coincide for larger values of W/H. Clearly, the shape of the strength curve for the ultimate S-shaped criterion does not agree with the empirical database. The mechanistic flaw in the envelope and the deviating strength suggests that the ultimate S-shaped criterion may not be suitable for modeling rock pillars in general.

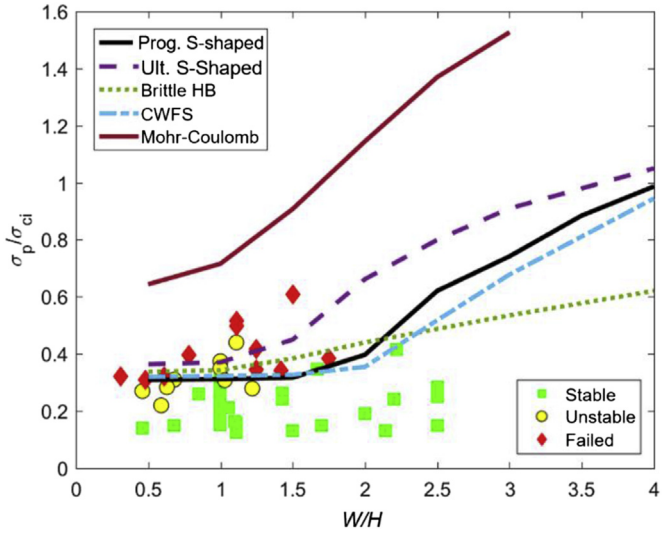

Fig. 4. Strength curves for different modeling techniques are overlaid on empirical pillar database. The empirical database was segregated for UCS of 200–300 MPa; the stable, unstable and failed case histories are denoted by green, yellow and red colors, respectively (modified from Sinha and Walton, 2018).

3.2. Mohr-Coulomb criterion with strain-softening

MC criterion is one of the earliest and widely recognized shear strength criteria in the field of rock mechanics. It relates the shear stress and normal stress at failure using two parameters: cohesion and friction angle (Jaeger and Cook, 1979). The simple linear relationship enables easy implementation in modeling software packages. FLAC^{3D} has a built-in strain-softening MC constitutive model that allows users to define residual cohesion and friction angle as a function of cumulative plastic shear strain (Itasca, 2016).

Field testing shows that pillars exhibit an overall strain-softening behavior. The similarity in shape with the FLAC^{3D} strain-softening constitutive model has often led to its use in past. It must, however, be recognized that the local (zone-scale) and the global (pillar-scale) responses are not always interchangeable – rather, an appropriate mechanistically accurate model applied at the zone-scale should lead to an emergent global behavior similar to what is observed in the field. The greatest disadvantage using a strain-softening MC criterion is its inability to account for the tensile spalling process. It is of interest, therefore, to test the outcomes of using such a criterion in modeling rock pillars. To that end, 6 models corresponding to *W/H* ratios of 0.5, 1, 1.5, 2, 2.5 and 3 were simulated using the geometrical setup as discussed in Section 2.

Fig. 2a illustrates the peak and residual MC envelopes used in the models. The two envelopes are coincident with the right portions of the peak and residual envelopes of the progressive S-shaped criterion, respectively. The peak envelope was degraded to the residual envelope over a plastic shear strain of 0.04 (the lag in the plastic shear strain between the peak and residual envelopes in the progressive S-shaped criterion was 0.05–0.01 = 0.04). Figs. 4 and 5 show the locus of the peak strength normalized to the UCS for different *W/H* ratios and the stress–strain curves for *W/H* ratios of 0.5, 1, 2 and 3, respectively. It seems that the peak strength increases in an exponential fashion, similar to what Iannacchione (1999) and Mortazavi et al. (2009) had observed from FLAC simulations. The reason for such an unrealistic trend is simply due to the fact that the low-confinement tensile spalling process was neglected. Even though this constitutive model captures the brittle to ductile transitional behavior in the stress–strain curves, it significantly overestimates the peak strength for squatter pillars.

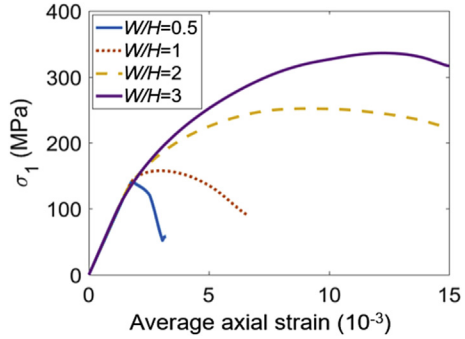

Fig. 5. Average stress–strain curves with W/H = 0.5, 1, 2 and 3 for the MC strain-softening models.

3.3. Brittle Hoek–Brown strength parameters

Like MC failure criterion, HB failure criterion is also one of the most commonly used strength envelopes in the field of rock mechanics. The major difference between the two criteria lies in their mathematical form in the principal stress space - MC is linear while HB criterion is nonlinear (Hoek et al., 2002). The convex shape of the HB envelope can be conceptually related to Patton's joint model (Patton, 1966). At lower confinement, there is a rapid increase in frictional strength due to interlocking of the asperities while at higher confinement, the cohesion increases rapidly due to shearing through intact material. With this conceptual framework and the knowledge that the surficial tensile fracturing is suppressed due to the generation of hoop stresses under uniaxial loading conditions, it can be understood that HB criterion only captures the shear failure mode of rocks. From this, it can be inferred that such a criterion, without any modification, would not accurately represent the progressive damage process in rock pillars.

Martin and Maybee (2000) proposed that initial (pre-peak) yield is governed by stress-induced spalling and that a shear failure plane develops only after the peak strength has been achieved. To capture this behavior, Martin et al. (1999) suggested the use of a set of brittle HB parameters, given by $m_b = 0$, $s = 0.11$ and $a = 0.5$. Plugging these values in the HB criterion gives the following equation:

$$\sigma_1 - \sigma_3 = 0.33UCS \tag{1}$$

The constant deviatoric strength equation assumes yield being dominated by cohesion. Although this may be true for slender pillars, it is generally not applicable to wider pillars where the strength is dominated by formation of confined cores where shearing mechanisms occur.

Six pillar models with *W/H* ratios of 0.5, 1, 1.5, 2, 3 and 4 were conducted with brittle HB parameters. The average stress–strain curves for *W/H* ratios of 1, 2, 3 and 4 are shown in Fig. 6. The flattened shape of the curves at higher axial strain is typically observed in models where the residual strength is equal to the peak strength. Clearly, this is not a realistic interpretation of how pillars behave when they are loaded in the field. When the strength locus is compared to the progressive S-shaped criterion in Fig. 4, the brittle HB predicts a slightly higher strength for W/H = 0.5–2 and a significantly lower strength for squatter pillars. The squatter pillar behavior is logical and can be due to the grounds of a lower initial and peak strength. The higher strength for slender pillars, on the other hand, is due to the absence of a residual envelope which underestimates the progressive damage localization process. Here the constant yield envelope (which is close to the CI threshold of the progressive S-shaped criterion) enables the stress-states of

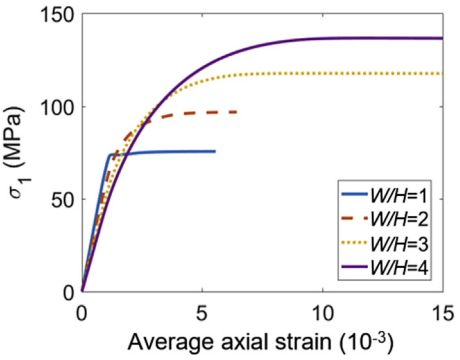

Fig. 6. Average stress–strain curves with $W/H = 1, 2, 3$ and 4 for the brittle HB models.

individual model zones to increase their minimum and maximum principal stresses, culminating in a slightly higher overall pillar strength.

3.4. Cohesion-weakening-frictional-strengthening (CWFS) model

The CWFS model was originally conceived by Schmertmann and Osterberg (1960) based on studies in clay. More recently, Hajiabdolmajid et al. (2002) introduced the CWFS strength model for capturing brittle failure in rocks. The driving force behind the development and extension of this model to rocks was the inability to replicate tensile-driven failure processes using conventional shear yield criteria (Pelli et al., 1991; Castro et al., 1995; Martin, 1997).

The CWFS model has been utilized by numerous authors to model the extent and shape of notches that typically form along the boundary of excavations in brittle rock (Hajiabdolmajid et al., 2002; Edelbro, 2009; Walton et al., 2015; Walton and Diederichs, 2015b). Walton et al. (2016) back-analyzed the pillar deformation in a hard rock mine in Sudbury, Canada using a combination of the CWFS strength model and the WD dilation angle model. The model was able to replicate the increasing confinement around the pillar core, pre-peak hardening in the average stress–strain curve, and formation of damage at low confinement regions within the pillar. The results of the study would seem to suggest that the CWFS strength model is capable of capturing the behavior of rock pillars. The key caveat applied in that study, however, is the low width to height ratio (~1.5) of the modeled mine pillar. The low confinement damage processes captured by the CWFS strength model are restricted to lower W/H ratios. For higher W/H ratios, the strength is governed by the formation of a confined core and this is expected to cause a deviation between the progressive S-shaped criterion and the classical CWFS model results.

To allow for a direct comparison, six pillar models were performed with W/H ratios of 0.5, 1, 1.5, 2, 2.5 and 3. The peak and residual envelopes (Fig. 2a) were introduced in the FLAC^{3D} model using the strain-softening MC constitutive relationship. The left portions of the yield and peak envelopes of the progressive S-shaped criterion correspond to the peak and the residual envelopes of the CWFS model in Fig. 2a.

The CWFS strength envelope was transitioned from peak to residual envelope over a cumulative plastic strain of 0.01. Fig. 7a shows the average stress-strain plot for W/H ratios of 0.5, 1, 2 and 3. Similar to MC model, the CWFS model captures the brittle to ductile transition behaviors of pillars. The average strength curve is very similar to the progressive S-shaped criterion models up to W/H ratios of 1.5, beyond which it falls (see Fig. 4). Intuitively, one would expect the strength would be higher because the ultimate strength envelope of the CWFS model is much higher than that of progressive S-shaped criterion under high confinement conditions.

To physically understand the reason behind this anomaly, the stress states for all elements in the $W/H = 3$ model were plotted in Fig. 7b. The near-horizontal alignment of the highly stressed elements was at first surprising; on coloring the elemental stress states on the basis of plastic shear strain, it was found that such an alignment was an artifact of the evolving nature of the envelope and the WD dilation model. The key difference between CWFS and progressive S-shaped criterion is the absence of the modified Mogi's line. The modified Mogi's line enables elements to be stressed at higher confinements without actually undergoing any yield. Since such is not the case with CWFS, yield and associated reduction in dilation angle occur earlier during the loading phase, causing the strength to fall below the progressive S-shaped model strength curve for squatter pillars. Additional research is necessary to determine the reason behind the similar trend in strength between CWFS and the progressive S-shaped criterion.

4. Effect of dilation angle model

The success of numerical models in replicating the behaviors of mine-scale structures is dependent on the choice of a yield criterion as well as a dilation angle model. The importance of capturing the mobilized nature of dilation angle has been the focus of limited studies (e.g. Zhao et al., 2010; Walton et al., 2015). Studies like Chugh and Abbasi (2012), Edelbro (2009) considered a constant zero dilation angle while Martin and Maybee (2000), Mortazavi et al. (2009), Kaiser et al. (2011), and Renani and Martin (2018) did not provide any information on the dilation angle used in

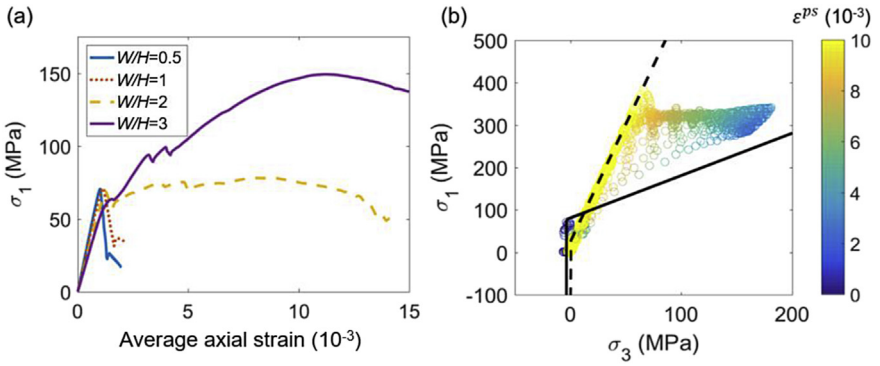

Fig. 7. (a) Average stress–strain curves with $W/H = 1, 2, 3$ and 4 for the CWFS model. (b) Elemental stress states colored by plastic shear strain (millistrain) for the CWFS $W/H = 3$ model.

their studies. It appears that the effect of dilation angle on the meso-scale behavior and its emergent effect on the overall model response have often been overlooked. Accordingly, in this study, a comparison of model responses obtained for different choices of dilation angle was performed, with a focus on pillar strength and damage mechanisms.

4.1. Comparison of mobilized and constant dilation angle results

Dilation angle plays an important role in the damage localization process as pillars are subjected to increasing load. With onset of inelastic deformation, inelastic lateral strains develop which in turn increase the confinement and strength of neighboring elements. Although localized, this phenomenon can significantly affect the global behavior of pillars (Walton, 2014). The magnitude of lateral plastic strain is controlled by the dilation angle that mathematically relates the plastic axial and lateral strain increments, given by (Vermeer and De Borst, 1984):

$$\dot{\varepsilon}_3^p/\dot{\varepsilon}_1^p = (\sin\psi + 1)/(\sin\psi - 1) \quad (2)$$

where $\dot{\varepsilon}_1^p$ and $\dot{\varepsilon}_3^p$ are the plastic strain rates in the major and minor principal directions, respectively; and ψ is the dilation angle. Several studies have found that the dilation angle is a function of confining stress and plastic shear strain and can be better represented by a mathematical model (Alejano and Alonso, 2005; Zhao and Cai, 2010; Walton and Diederichs, 2015a).

The most relevant study in literature which has considered the influence of dilation angle on pillar behavior is that by Walton et al. (2015), who looked into the differences in damage localization, confining and vertical stresses on a horizontal cross-section along the mid-height of granite pillars. Results indicated that the use of a 0° dilation angle underestimates the confining and vertical stresses through the cores of pillars. This observation is intuitive since dilation angle of zero minimizes the right hand side of Eq. (2), producing the least increase in plastic confining strain. Another set of models in Walton and Diederichs (2015a)'s study utilized a constant 30° dilation angle, as a simplifying approximation to the mobilized WD dilation angle model. This also generates contours of plastic yield, vertical and confining stresses, highly dissimilar to those obtained using the mobilized WD dilation model. Clearly, the use of a constant dilation angle is not sufficient in describing the complex interdependence of dilatancy and damage on overall model response.

In this study, the W/H ratios of the pillars were varied from 0.5 to 4 with four choices of dilation angle: (a) WD model, (b) $\psi = 0°$, (c) $\psi = 15°$, and (d) $\psi = 30°$. The model geometry and loading conditions are similar to those described in Section 2. Fig. 8a and b shows the pillar strength as a function of W/H and the stress–strain curves for $W/H = 2$ and 3 with WD, $\psi = 0°$ and $\psi = 15°$ models, respectively.

The trends in pillar strengths for all the models are consistent with the sigmoid shape, as previously illustrated in Fig. 4. It can therefore be concluded that the distinct form of the curve is a manifestation of the progressive S-shaped criterion, rather than the WD dilation model. For slender pillars, the peak strengths are comparable regardless of the dilation model used; the discrepancies between the different cases widen with increased W/H ratio. Mechanically, failure in slender pillars is governed by the formation of a cross-shear plane, where dilation angle does not play any significant role. With increase in the W/H ratio, a confined core develops as a response to the dilation of failed peripheral elements. It is under these confinement conditions that the choice of dilation angle has the greatest impact. In terms of the stress–strain curves, the $W/H = 3$ model with zero dilation angle showed a distinctly different trend. The higher strength for the $\psi = 0°$ model (also see Fig. 8a) seems to contradict the general notion that reducing the dilation angle reduces the plastic strain-generated confinement in the core, leading to an overall lower strength. This also contradicts the lower confining stresses observed in pillar simulations of Walton et al. (2015). This leads one to question whether the pillar strength decreases or increases with reduction in dilation angle as well as what causes the discrepancy in the observed pillar behavior.

4.2. Damage processes for different dilation angles

The stress–strain curves shown in Fig. 8b provide a reasonable explanation to the questions raised above. In addition to higher overall strength, both the $W/H = 2$ and 3 ($\psi = 0°$) models exhibited a delayed strength mobilization, i.e. the models underwent a much larger amount of strain before the peak strength was reached. At an intermediate axial strain level (0–0.005 for $W/H = 2$ and 0.005–0.01 for $W/H = 3$), the average stress in the models with WD and $\psi = 15°$ was actually greater. It is therefore likely that the confining and vertical stress plots in Walton et al. (2015) were generated at a stage when the average stress of the $\psi = 0°$ model was below that of the WD model. This reasoning can be applied to Creighton pillar ($W/H = 1.5$) since a delayed strength mobilization was also observed in the $W/H = 1.5$ model (similar to $W/H = 2$ model as shown in Fig. 8b). If the loading in Walton et al. (2015) was continued, the stresses in the zero dilation model may have eventually exceeded the WD pillar stresses.

To better understand this phenomenon, the plastic shear strain and confining stresses for $W/H = 3$ model were plotted in Fig. 9. The plastic shear strain contours in Fig. 9a and b are for WD and $\psi = 0°$ model respectively at a solution step when the WD model reached

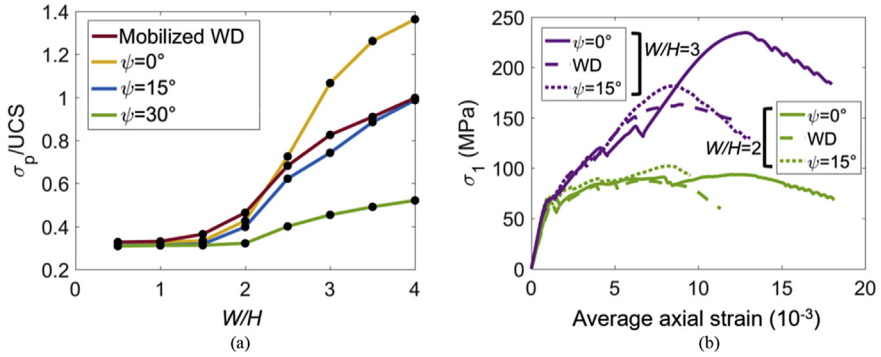

Fig. 8. (a) Variation in strength with W/H ratio for different dilation angles, and (b) stress–strain curve for $W/H = 2$ and 3 with WD model, $\psi = 0°$ and $\psi = 15°$.

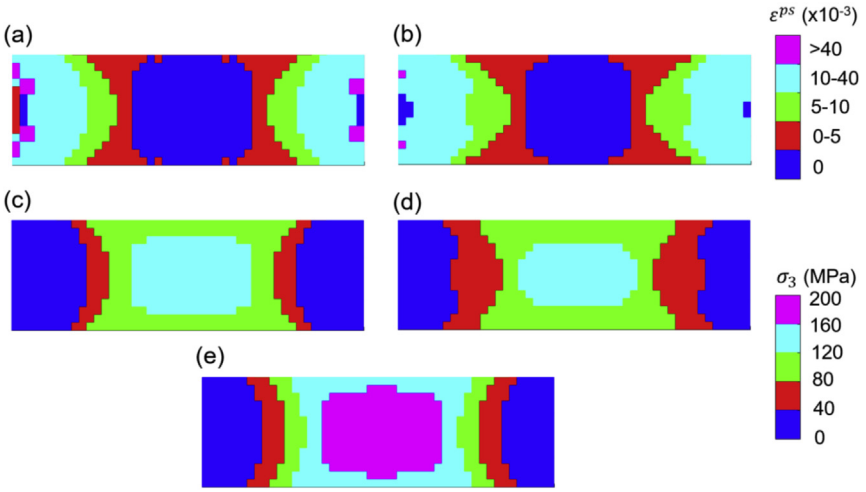

Fig. 9. Plastic shear strain contours for $W/H = 3$ with (a) WD model; and (b) $\psi = 0°$; Confining stress contour for $W/H = 3$ with (c) WD model; and (d) $\psi = 0°$ at a solution step when the WD model reached its peak strength; and (e) Confining stress contour for the $\psi = 0°$ model when it reached its peak strength.

its peak strength. The confining stress contours in Fig. 9c and d are located at the same solution step. Fig. 9e shows the confining stresses at the solution step when the $\psi = 0°$ model reached its peak strength. Surprisingly, when the WD model reached its peak strength, the volume of plastic yield in the core was lower than that in the $\psi = 0°$ model. Laboratory tests on granitic and sedimentary rocks have shown the dilation angle to decrease with increases in confinement and plastic shear strain (Walton and Diederichs, 2015a). Ideally in a pillar, the peripheral elements are supposed to dilate first, followed by a load transfer to the central portion/core and ultimate dilation of the pillar core. The shedding of load due to yielding of the pillar core should be concurrent with the first major fall in the stress–strain curve from the peak.

The sequence of compression and dilation that occur in the pillar core with progressive loading is severely delayed when a dilation angle of zero is chosen in a numerical model. For example, dilation angles of 15°, 30° and 45° yield 1.7, 3 and 5.8 respectively as a plastic strain increment ratio (right side of Eq. (2)). A dilation angle of zero assumes the multiplier to be 1, severely underestimating the amount of lateral plastic strain (and confinement) generated for a unit change in vertical plastic strain. Physically, this means that as the core of the $\psi = 0°$ model yields, it dilates marginally, preventing the core from shedding its confinement. With further damage accumulation and confinement build-up, the stress in the core increases to a much higher value (see Fig. 9e) in comparison to WD/constant non-zero dilation models.

Given the similarity in the stress–strain curves for WD and $\psi = 15°$ model, it seems that a single value can replicate the response of a mobilized dilation model. This could be partly due to the rapid mobilization (γ_m) of dilation angle and its relative insensitivity to confining stress (for crystalline rocks), enabling a non-zero dilation angle to reasonably approximate the mobilized model. Since this approach is only approximate, the stress–strain curves as well as the variation of strength with W/H ratios do not match perfectly with the WD model results. Although such a difference may be negligible from a practical perspective, the authors would like to point out that the emergent macro-behavior could be significantly different in softer materials. Wherever possible, a mobilized dilation model should be used for simulating excavation-scale structures.

5. Random assignment of strength parameters

The previously mentioned studies have all assumed model elements to have a uniform constitutive behavior. In reality, most rock masses are heterogeneous on a scale that depends on its origin and constituent minerals. When such a rock mass is assigned with uniform strength in a continuum model, it is implicitly assumed that the meso-scale variability in material property can be adequately represented by an equivalent homogenous medium. While such a simplistic approach has been proven to be effective (Edelbro, 2009; Sinha and Chugh, 2016; Walton et al., 2016), it does not consider the potential effects of areas with heterogeneous strength characteristics to control post-yield localization, and ultimately, pillar strength and brittleness.

Unlike grain-based modeling (Lan et al., 2010; Nicksiar and Martin, 2012; Ghazvinian et al., 2014), FLAC^{3D} does not possess the capability to simulate discrete grains. Thus, the primary option for simulating heterogeneity is to assign probability distributions to the principal input parameters of a yield criterion and randomly allocate the properties in a model. This approach is in no way comparable to grain-based modeling because the variability in strength is only modeled at the element scale (0.166 m in this case). Due to computational constraints, the element sizes used for modeling mine-scale structures are much larger than that of typical grains. Therefore, this randomized approach only serves as an assessment of the model's sensitivity to meso-scale heterogeneity in mechanical properties.

The authors would like to note here that although some studies (e.g. Tang, 1997; Guo et al., 2017) have been performed on methodologies for stochastic modeling of rock properties, they are not directly relevant to this current study due to two primary reasons: (1) The objectives of the referenced studies were to indirectly model the progressive failure behavior of rocks by incorporating heterogeneity in rock strength properties. In contrast, the failure process is explicitly represented here by the progressive S-shaped yield criterion and WD dilation angle model. This study's goal with respect to stochastic modeling is to assess the model's sensitivity to meso-scale variations in mechanical properties (related to the stochastic nature of the damage thresholds measured in laboratory). (2) In the referenced studies, a Weibull or Gaussian distribution was employed for representing rock strength heterogeneity.

With an increase in heterogeneity, a lower global strength was observed and this could be related to the larger number of weaker elements in the model. In this study, the friction angle and cohesion of different segments of the progressive S-shaped criterion were assigned independently (following a Gaussian distribution). This means that a higher coefficient of variation (CV) does not necessarily imply an increase in the number of weaker elements in the model (for example, one element might have a lower ϕ for CD but a higher ϕ for CI, where ϕ is the friction angle) – the behavior is far more complex. Consequently, a direct comparison between the results presented in this study and those in the referenced studies is not appropriate.

Following the finding of Langford and Diederichs (2015), a Gaussian distribution was assigned to the different parameters of the progressive S-shaped criterion. The mean cohesion and friction angle values were chosen from Table 1, and the CV values of 5% and 10% were used. Fifteen realizations of $W/H = 1$, 2 and 3 pillars were performed with each set of parameters. Fig. 10 shows the model distribution of initial cohesion with $CV = 5\%$ and 10%.

The progressive S-shaped criterion has 14 input parameters: 6 cohesion values, 6 friction angle values and 2 plastic shear strain values. When developing these models considering heterogeneity, two decisions were made: (a) the intersection point of the low and high confinement portions would be kept consistent for all three envelopes, and (b) the three envelopes would coincide for some constant values of confinement. The two constraints reduce the degrees of freedom such that the entire criterion can be defined by using only 12 principal parameters. Outlined below are the steps that were followed for developing the models:

(1) For every model element, first a random friction angle and a cohesion were selected from the Gaussian distributions for the left and right sides of the peak envelope. The confinement level separating the left and right segments of the progressive S-shaped criterion was then computed.
(2) Next, the cohesion of the left side and the friction angle for both sides of the yield envelope were selected. The cohesion for the right side of the yield envelope could then be calculated to ensure the same intersection point of the low and high confinement portions of the yield envelope as for the peak envelope. This then constrained the confining stress point at which all three envelopes would coincide.
(3) Finally, the cohesion and friction angle of the left side of the residual envelope were extracted from the Gaussian distribution. The right segment of the residual envelope was then calculated based on the two constraints as stated above.

The stress–strain curves for $W/H = 1$ and 3 with $CV = 5\%$ and 10% are shown in Fig. 11. The variability in the peak strength and the post-peak behavior increases with increasing CV values. This is an intuitive result, given the wider range of plausible input parameters. The degree of ductility is also affected by the variability in input properties. For example, in Fig. 11d, there are clear variations in ductility, and no consistent relationship between changes in strength and ductility/brittleness is observed. For $CV = 5\%$, the shape of the post peak-portion is very similar in all cases.

The plastic shear strain distribution in the deterministic model for the same solution steps was obtained (Fig. 12a and b). In order to investigate how the property differences in spatial variability could affect the micro-damage process, plots of plastic shear strain for two solution steps (separated by 1000 steps) were also generated, as shown in Fig. 12c and d. A narrow color range for the plastic shear strain was chosen to readily identify the onset of yield for different model elements. The differences between the stochastic and deterministic models for step X and step $X + 1000$ are apparent from Fig. 12a–d. The plastic shear strain distribution (Fig. 12a and b) is almost unchanged over the range of steps considered for the deterministic model, implying no additional yielding over 1000 steps. Given the same applied strain path, the dissimilar pattern between the stochastic and deterministic models at step X could only be justified on grounds of variation in strength properties. Over the 1000 steps, the number of yielded elements was increased by six in the plot of the stochastic model yield. This is apparently in contrast to what was observed for the deterministic model.

Fig. 12a–d only depicts the differences between the stochastic and deterministic models at early stages of loading. To observe the relative differences at a late loading phase (i.e. closer to the pillar peak strength), plastic shear strain contours were generated for the two models (Fig. 12e and f). The colorscale was modified such that blue represents 'no yield', red represents 'at/beyond yield envelope but not close to peak envelope', green represents 'beyond yield envelope and close to peak envelope', cyan represents 'beyond peak envelope but not close to residual envelope' and magenta represents 'close to or at residual envelope'. The larger proportion of yielded elements in the core indicates that damage propagated faster in the stochastic model. Furthermore, the proportion of yielded elements closer to the peak envelope (i.e. green) also seems to be much larger in the stochastic model. Clearly, the mesoscopic yielding process has a significant effect on the overall model response.

Fig. 13a and b shows the mean, standard deviation (SD) and the CV of the model strengths. The mean values correspond fairly well with those of the deterministic models ($W/H = 1$: 0.31; $W/H = 2$: 0.4; $W/H = 3$: 0.74). With an increase in the CV of the

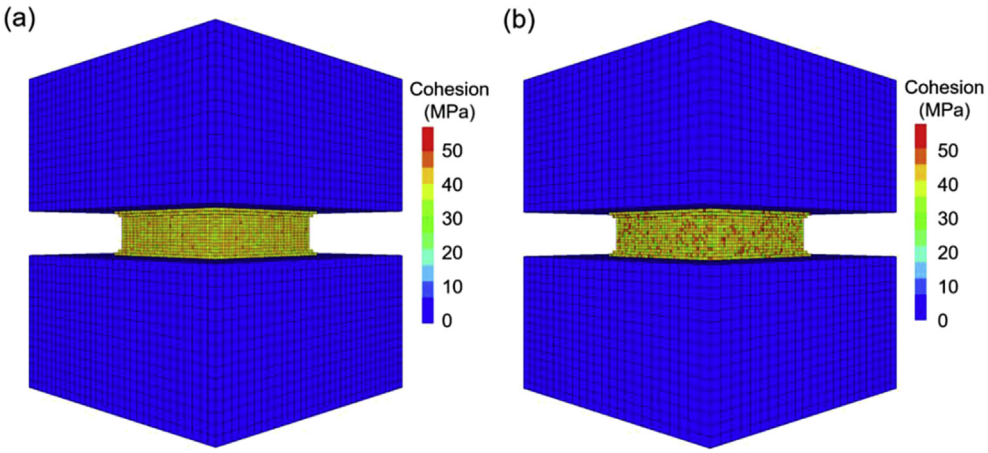

Fig. 10. Cohesion distribution for $W/H = 3$ model with (a) $CV = 5\%$, and (b) $CV = 10\%$.

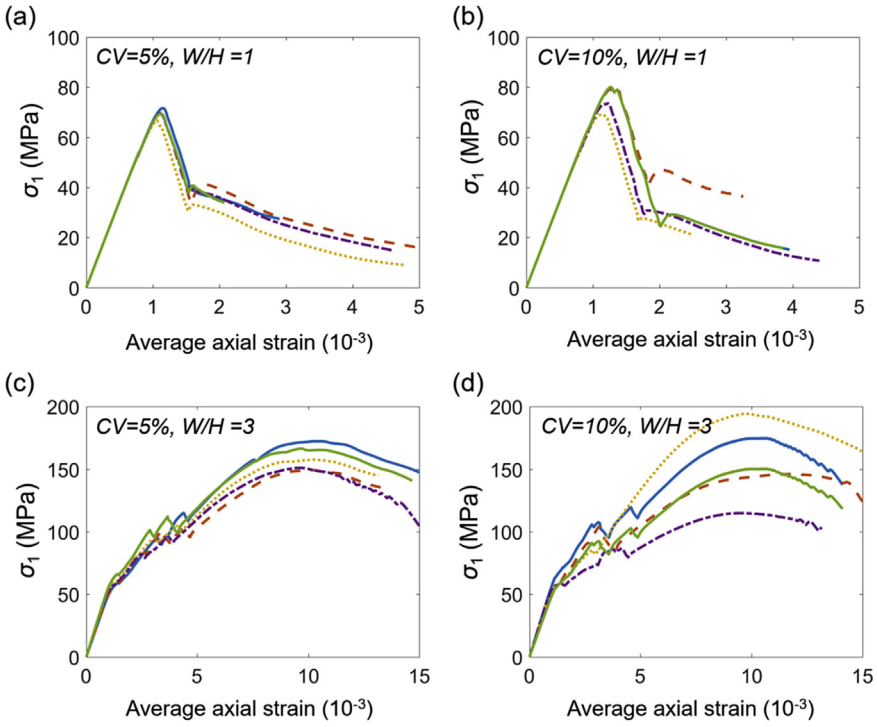

Fig. 11. Stress–strain curves for (a) $CV = 5\%$, $W/H = 1$; (b) $CV = 10\%$, $W/H = 1$; (c) $CV = 5\%$, $W/H = 3$; and (d) $CV = 10\%$, $W/H = 3$.

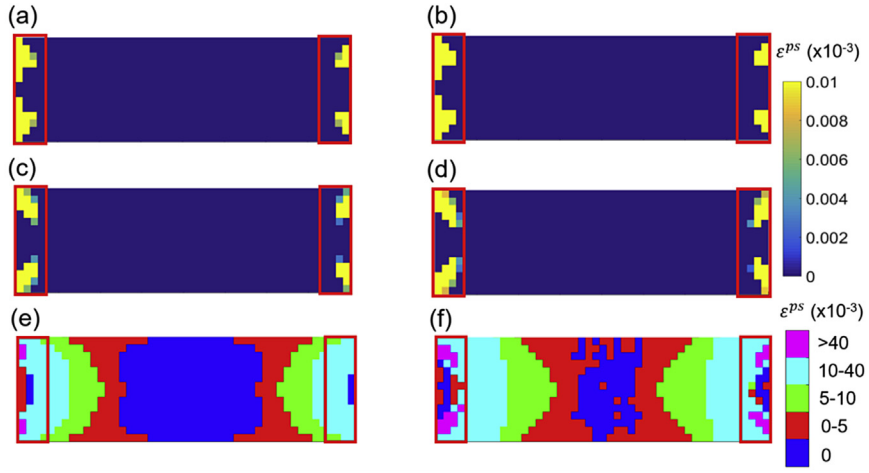

Fig. 12. Contours of plastic shear strain for deterministic $W/H = 3$ model at (a) step X, (b) step $X + 1000$; for the stochastic standard deviation ($SD = 10\%$) model at (c) step X, (d) step $X + 1000$; (e) ε^{ps} distribution for deterministic model at a solution step near model peak strength; and (f) ε^{ps} distribution for stochastic model at the same solution step as that in (e).

principal input parameters, the SD of the pillar strength increased. However, since the means are different, it is more appropriate to compare CV values instead of SD values. The $W/H = 1$ model exhibited a brittle behavior with a consistent mean and a very low CV. Such slender pillars do not develop any confined core and typically fail through formation of through-going shear planes. The $W/H = 2$ models, on the other hand, exhibited a significantly higher CV in comparison to $W/H = 3$ for both sets of models. This was in contrast to the authors' expectation that the variation in the macro-strength should increase as the pillar becomes squatter. With 15 realizations performed for each set of model, the trend obtained is not a consequence of insufficient data points, and a mechanistic explanation must exist that can justify this trend.

Upon inspection of the post-peak portion of the stress–strain curves, it was observed that some of the $W/H = 2$ models failed in a brittle fashion while others exhibited a more ductile behavior, including pre-peak hardening to a higher peak strength value (see Fig. 13c). However, none of the $W/H = 1$ or 3 models showed such variations in macro-failure mode. The only logical explanation then is that $W/H = 2$ pillar is near the brittle to ductile transition point (for this particular rock type) and slight variations in the distribution of material properties led to either a brittle, a perfectly plastic or a strain-hardening behavior. This explains the scenario that the CV value for $W/H = 2$ models is significantly larger than that for $W/H = 3$.

For the granite pillar studied, a deterministic approach seems acceptable given the similar average peak strength and post-peak

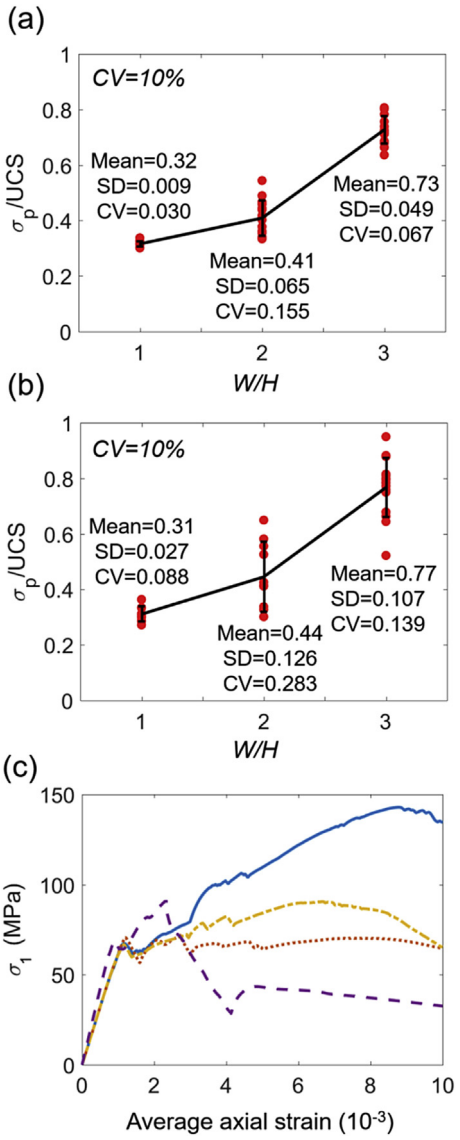

Fig. 13. Error bar plot (1 SD on either side of the mean) of normalized peak strengths for (a) $CV = 5\%$ with 15 data points, (b) $CV = 10\%$ with 15 data points, and (c) Average stress–strain curves for $CV = 10\%$, $W/H = 2$ models.

behavior to those observed from the stochastic models considering heterogeneity. The fluctuation in the failure mode for $W/H = 2$ does suggest the potential application of the stochastic modeling of pillar stability, especially when many mine pillars are designed with W/H ratios around 2. Rock masses are heterogeneous by nature, and capturing the spatial variability in material strength becomes critically important for design purposes. The advantage of simulating different realizations with variable material strengths is that a range of factors of safety or other indicators in terms of stability could be obtained. This could help in design of underground structures considering the worst case scenario. Although this study used the findings of Langford and Diederichs (2015) to assign a CV to the principal input parameters, other researchers should strive to estimate the site-specific values from laboratory testing.

6. Effect of length on pillar strength

Rectangular pillars are used in various mines because of the three associated advantages: (a) It can alleviate roof stress under high horizontal stress conditions by minimizing the area of exposed roof (Dolinar and Esterhuizen, 2007), (b) it improves mine ventilation by minimizing leakages (Grau et al., 2006) and head losses at corners, and (c) smaller numbers of cross-cuts reduce the number of required ventilation terminations. From both production and safety points of view, longer pillars can aid in rapid completion of the development phase of mining and provide greater stability to openings that must remain functional throughout the life of the mine. Bearing in mind these numerous benefits, it is important to quantify the improvement in stability that can be achieved by varying the pillar length.

To date, the number of studies conducted on width effect far supersedes the studies undertaken to investigate the effect of pillar length on pillar behavior. It has basically been hypothesized in the past that pillar strength is governed by its shorter dimension; consequently, most of the empirical equations do not account for the 'length' term. While this may be true for slender pillars, it is clearly erroneous for squatter pillars where the strength is controlled by the volume of the confined pillar core. With the validity of the progressive S-shaped criterion as well as the modeling approach established, it was possible to extend the models tested in this study to evaluate this effect.

6.1. Background

There are five prominent studies conducted on the effect of pillar length on pillar strength over the years. The most recent one by Dolinar and Esterhuizen (2007) discussed the Bauschinger-Johnson (Babcock, 1994), Mark-Bieaniawski (Mark, 1990; Mark and Chase, 1997), Grobbellar and Wagner equations (Wagner, 1980) and the potential issues that can arise in applying them to rock pillars. Recognizing the strengthening effect of pillar length, Wagner (1980) introduced the concept of effective width given by

$$w_{\text{eff}} = \frac{4A_{\text{p}}}{C} \tag{3}$$

where A_{p} is the area and C is the circumference of the pillar. For a square pillar, w_{eff} reduces to the width of pillar; while with increasing length, w_{eff} approaches a constant value of $2W$, where W is the width. Physically, this implies that the rate of increase in strength tapers for longer pillars and beyond a point, the improvement is negligible. Such a trend is demonstrated by the models presented by Dolinar and Esterhuizen (2007). The Mark-Bieniawski equation is a modified version of the Bieniawski equation which analytically computes the ultimate strength by integrating the vertical stress gradient given by Wilson (1983). Since the parameters were developed specifically for squatter coal pillars, it is unsuitable for estimating the strength of rock pillars in general.

Dolinar and Esterhuizen (2007) used FLAC^{3D} models to investigate the effect of length using two different yield criteria: a strain-softening MC criterion and a brittle strength criterion. An array of models was simulated for L/W (L is the length) ratios of 1–6 and W/H ratios of 0.5–1.5. Results showed that increasing the length substantially increased the strength of squatter pillars but had negligible impact on slender pillars.

To justify the results on mechanistic grounds, Dolinar and Esterhuizen (2007) computed a confining stress factor for each model. The hypothesis was that the overall strength of a rectangular pillar was simply an addition of the strength of the 'pillar ends' and the 'central core' (measured as confining stress factor). It was found that for slender pillars, the core factor was very low which led to the conclusion that height was a dominant factor in those cases. For the squatter pillars, there was an initial increase in the core factor, followed by tapering beyond $L/W = 5$.

This study was the first systematic investigation designed to critically analyze the effect of pillar length. However, since the manner in which the brittle strength criterion was defined is incomplete, the results may not be entirely representative of the true physical process.

6.2. Numerical investigation of L/W effect

A set of 30 pillar models corresponding to W/H ratios of 0.5, 1, 1.5, 2, 3, and 4, and L/W ratios of 1, 2, 3, 4, and 5 was used for this study. With all material parameters and boundary conditions held constant (as per the Creighton granite case), modifications were made only to the length of the models as discussed in Section 2. Fig. 14 shows the average stress–strain curves for L/W ratios of 2 and 4. Apart from the similar brittle to ductile transitive behavior in both sets of models, the moderate strength increase associated with length is clearly perceptible. The W/H ratio has a greater influence on the pillar strength than the L/W ratio.

Because the strength for the L/W models exhibited an S-trend, a sigmoidal function was chosen to fit the data points (Table 3) and is given by Eqs. (4) and (5). A three-dimensional (3D) surface plot of the derived equation is also presented in Fig. 15. Although the fitted equation may be of little practical usage, it manages to capture the relatively uniform strength for $W/H = 0.5–1.5$ and the non-negligible effect of L/W on strength for squatter pillars. A multi-regression analysis with interaction terms, on the other hand, generated a simpler mathematical relationship but failed to capture the S-shape.

$$\frac{\sigma_p}{UCS} = 0.3 + \frac{0.725}{1 + e^{6.78-2.41W/H}} + m\ln(L/W) \tag{4}$$

$$m = -0.01 + \frac{0.14}{1 + e^{11.35-6.07W/H}} \tag{5}$$

where σ_p is the pillar strength in MPa; and L, H, and W are in m.

When applying Eqs. (4) and (5), it must be noted that this study only considered pillars where the W/H and L/W are in the ranges of 0.5–4 and 1–5, respectively. The logarithmic relationship of L/W ratio to the strength is consistent with the findings of Ryder and Ozbay (1990), Dolinar and Esterhuizen (2007) and the effective width concept of Wagner (1980). A similar diminished length effect for $L/W > 4$ on strength was also predicted by Ryder and Ozbay (1990) and Dolinar and Esterhuizen (2007).

From Table 3, it can be seen that with increase in length, the strength reduces for W/H rations of 0.5 and 1 while it increases for the other considered ratios. To comprehend the reason for such a behavior, the volumetric core proportion for each of the model was computed. This was done on grounds similar to Dolinar and Esterhuizen (2007), following the suggestion of Valley et al. (2011) that the confinement level corresponding to the intersection of the CI and spalling limit could be used as a demarcation between the outer and inner shells. In our cases, the point of intersection was 12.4 MPa, suggesting that the elements in the

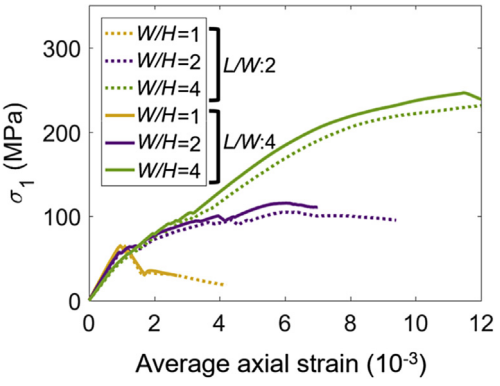

Fig. 14. Average stress–strain curves for $W/H = 1$, 2 and 4 and $L/W = 2$ and 4.

Table 3
Normalized peak strength for the 30 models performed as a part of this study.

L/W	Normalized peak strength					
	W/H = 0.5	W/H = 1	W/H = 1.5	W/H = 2	W/H = 3	W/H = 4
1	0.31	0.31	0.31	0.4	0.74	0.99
2	0.3	0.31	0.31	0.48	0.83	1.08
3	0.29	0.3	0.32	0.51	0.9	1.13
4	0.29	0.29	0.33	0.53	0.93	1.17
5	0.3	0.29	0.33	0.53	0.94	1.2

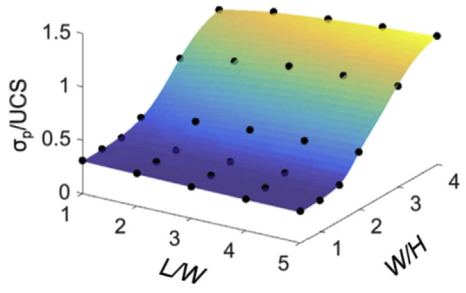

Fig. 15. Fitted surface shown in 3D with model predicted strength as black dots.

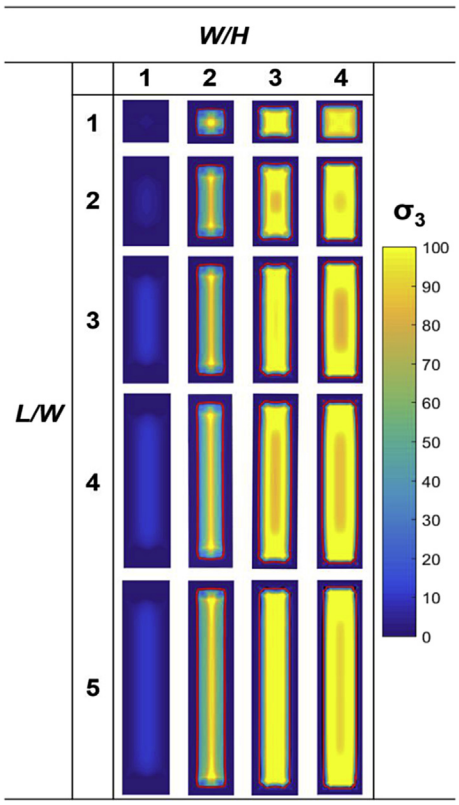

Fig. 16. Contour of σ_3 (in MPa) along horizontal cross-section of the models. The black line marks the boundary of the core.

pillar which exceeded this value were considered as a part of the pillar core. The core proportions were determined at the solution step where the respective models achieved their peaks.

Fig. 16 and Table 4 show the horizontal pillar sections and the volumetric core proportion for each of the models, respectively. The red contour lines in the sections characterize the boundary between the outer and inner shells. In case of W/H of 1, no element along the mid-section had a confinement level higher than 12.4 MPa.

In slender pillars, the core proportions are low (<25%) and reduce further with an increase in length. The number of elements constituting the core increases with length but when normalized to the total volume, it shows a decreasing trend. To illustrate why this occurs, the confining stress contours along two vertical sections were prepared at distances of 4 m and 8 m from the pillar end for the $W/H = 1$, $L/W = 4$ model (see Fig. 17). It can be seen that the elements which contribute to the core reduce along the length, consequently causing the normalized core proportion to decline.

Table 4
Volumetric core proportions for the 30 models.

L/W	Volumetric core proportion (%)					
	$W/H = 0.5$	$W/H = 1$	$W/H = 1.5$	$W/H = 2$	$W/H = 3$	$W/H = 4$
1	13.2	24.5	37.9	44.5	55.9	63.3
2	11.2	16.1	39.5	54.2	58.8	68.6
3	9.3	11.1	42.7	565	60.2	71.4
4	7.8	8.8	45.4	58.3	62.7	71.7
5	6.9	7.4	47.1	59.9	63.4	71.9

For squatter pillars, the spread of the shear plane across the entire width is restricted by the pillar height, enabling a confined core to form around the center. With increase in length, the longitudinal extent of the core is extended and this corresponds to an increase in the volumetric core proportion. Beyond the L/W ratio of ~3–4, the increase in the number of core elements is balanced by the rise in the total number of pillar elements. As a mathematical explanation, we have

$$\textit{Volumetric Core Proportion}\ (\%) = 100\frac{a + b(L-8)WH}{LWH} \tag{6}$$

where a is the volume of core for $L = 8$ m, and b is the fraction of the extra volume that contributes towards the core for lengths higher than $L = 8$ m (recall that $W = 8$ m is fixed in this case). Then Eq. (6) can be re-written as

$$\textit{Volumetric Core Proportion}\ (\%) = 100\left[\frac{a}{LWH} + b\left(1 - \frac{8}{L}\right)\right] \tag{7}$$

Differentiating both sides of Eq. (7) with respect to L, we have

$$\frac{\mathrm{d}(\textit{Volumetric Core Proportion})}{\mathrm{d}L} = \frac{100}{L^2}\left(8b - \frac{a}{WH}\right) \tag{8}$$

It becomes evident from the inverse square relation that as the length increases, the rate of increase in the volumetric core proportion reduces drastically. This simple analysis was conducted assuming that the proportion of extra elements contributing to the core is constant. This is a crude approximation made on the basis of vertical cross-sectional contour plots of confinement; nevertheless, it serves to justify the trend in Table 4.

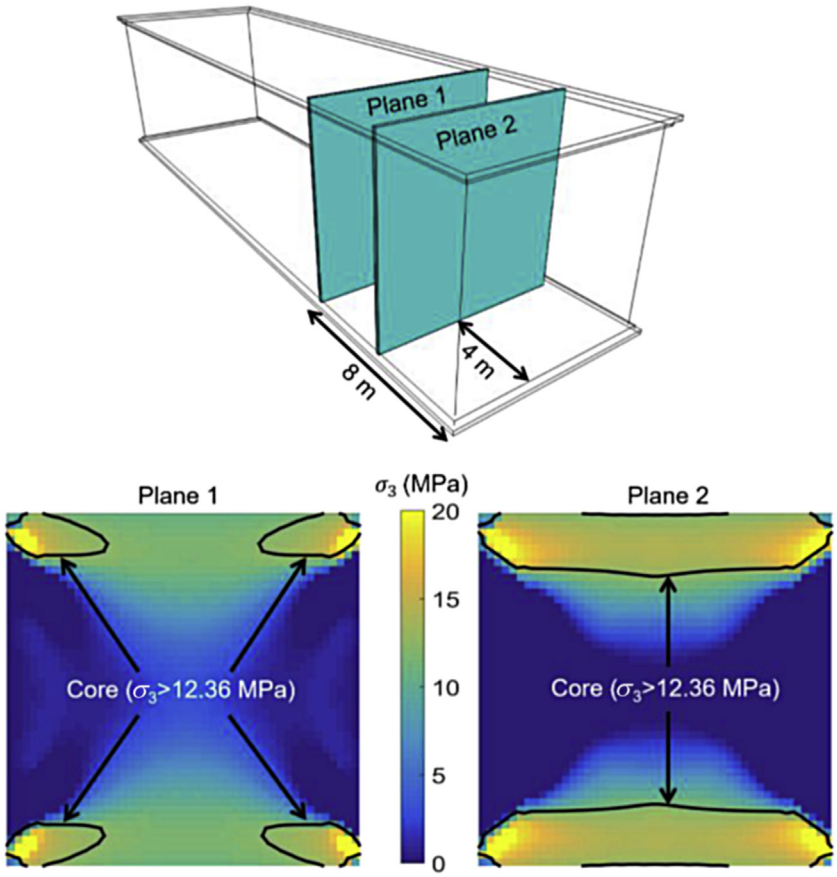

Fig. 17. Contours of confinement along vertical cross-section in $W/H = 1$, $L/W = 4$ model located at 4 m and 8 m from pillar edge.

The results obtained in this section substantiate the effect of length in improving the overall strength of pillars. The volumetric core proportion trend is similar to that obtained in Dolinar and Esterhuizen (2007). However, the sectional plot of confinement indicates that it may be erroneous to consider only the longitudinal ends of the pillars as inner shell (see Fig. 16), as was considered in Dolinar and Esterhuizen (2007). The overall strength and failure behavior are phased by tensile-driven shear in slender pillars and surficial spalling-confined core in squatter pillars. In the slender pillar case, the core formation is obscured by the effect of height, causing the strength to remain invariant with changes in length.

7. Conclusions

This study presented a comparative analysis between the progressive S-shaped criterion and four traditional yield criteria in modeling rock pillars, namely the brittle HB, CWFS, strain-softening MC and ultimate S-shaped criteria. While the progressive S-shaped criterion is more complicated than the others considered, it also more faithfully captures the range of failure mechanisms that occur in rocks (Sinha and Walton, 2018), and accordingly is a more useful tool for research. It was found that apart from CWFS, all the other criteria tended to overpredict the strength of hard rock pillars. The resemblance between the results of CWFS and progressive S-shaped criterion may be a consequence of the high brittle to ductile transition for the modeled granitic rock that prevented majority of the elemental stress states from transitioning to the right side of the yield criterion. As a result, the emergent model behavior using the two yield criteria were similar. Further study is required to ascertain how similar the results obtained using these two strength models might be under different conditions.

The choice of representation of dilation angle was shown to have a major effect on the overall model results. A zero dilation angle delayed the progression of the yield process, eventually overpredicting the pillar strengths. It was also found that an appropriate constant non-zero dilation angle can fairly approximate the complexity of a mobilized model. However, such may not be the case in other rock types, where use of a mobilized dilation model may be necessary.

Continuum modeling techniques generally employ an equivalent homogenous material to simulate heterogeneous rock masses. Although this approach has been proven to be useful, this study explored how spatial heterogeneity in micro-strength affects pillar behavior. It was found that for $CV = 5\%$ and 10% in input parameters, the $W/H = 1$ model exhibited a brittle behavior while $W/H = 3$ showed a ductile behavior. The most interesting observation was the variable failure mode for $W/H = 2$ model, indicating that $W/H = 2$ acted as a brittle to ductile transition point for the rock pillar in present study. From a mechanistic perspective, the failure localization at zone-scale was significantly different in comparison to the deterministic model. This led to a wide scatter in the peak pillar strength values. Nonetheless, the average peaks were similar between the deterministic and stochastic model sets. With the exception of $W/H = 2$, the post-peak behaviors were relatively consistent with those of the deterministic models as well. Given that the modeling approach used was found to be effective compared to the others considered, it was used to study the L/W effect on pillar strength. A modest increase in strength was noted, associated with an increase in volume of the confined core. The effect of length was minimal for slender pillars and was minimal beyond $L/W > 4$ for all cases.

Conflicts of interest

The authors wish to confirm that there are no known conflicts of interest associated with this publication and there has been no significant financial support for this work that could have influenced its outcome.

Acknowledgement

The research conducted for this study was funded by The National Institute for Occupational Safety and Health, USA (NIOSH) (Grant No. 200-2016-90154). The authors would like to extend their sincere gratitude for this financial support.

References

Alejano LR, Alonso E. Considerations of the dilatancy angle in rocks and rock masses. International Journal of Rock Mechanics and Mining Sciences 2005;42(4):481–507.
Babcock C. Critique of pillar design equations from 1833 to 1990. Denver, CO: U.S. Department of the Interior, Bureau of Mines; 1994. IC 9398.
Bahrani N, Kaiser PK, Valley B. Distinct element method simulation of an analogue for a highly interlocked, non-persistently jointed rockmass. International Journal of Rock Mechanics and Mining Sciences 2014;71:117–30.
Castro L, McCreath D, Kaiser PK. Rockmass strength determination from breakouts in tunnels and boreholes. In: Proceedings of the 8th ISRM congress. Tokyo, Japan: International Society for Rock Mechanics and Rock Engineering; 1995. p. 531–6.
Chugh YP, Abbasi B. A numerical analysis of a four-way coal mine intersection with primary and secondary supports. In: Proceedings of the 12th ISRM congress. Beijing, China: International Society for Rock Mechanics and Rock Engineering; 2012. p. 363–8.
Diederichs MS. Rock fracture and collapse under low confinement conditions. Rock Mechanics and Rock Engineering 2003;36:339–81.
Diederichs MS. The 2003 Canadian Geotechnical Colloquium: mechanistic interpretation and practical application of damage and spalling prediction criteria for deep tunnelling. Canadian Geotechnical Journal 2005;44(9):1082–116.
Diederichs MS, Martin CD. Measurement of spalling parameters from laboratory testing. In: Rock mechanics in civil and environmental engineering. London: Taylor & Francis Group; 2010. p. 323–6.
Dolinar DR, Esterhuizen GS. Evaluation of the effect of length on the strength of slender pillars in limestone mines using numerical modeling. In: Proceedings of the 26th international conference on ground control mining. Morgantown, WV: West Virginia University; 2007. p. 304–13.
Edelbro C. Numerical modelling of observed fallouts in hard rock masses using an instantaneous cohesion-softening friction-hardening model. Tunnelling and Underground Space Technology 2009;24(4):398–409.
Edelbro C. Different approaches for simulating brittle failure in two hard rock mass cases: a parametric study. Rock Mechanics and Rock Engineering 2010;43(2):151–65.
Esterhuizen GS. Combined point estimate and Monte Carlo techniques for the analysis of wedge failure in rock slopes. In: Statics and dynamic consideration in rock engineering. Rotterdam: A.A. Balkema; 1990. p. 125–32.
Farahmand K, Diederichs MS. A calibrated synthetic rock mass (SRM) model for simulating crack growth in granitic rock considering grain scale heterogeneity of polycrystalline rock. In: Proceedings of the 49th U.S. rock mechanics/geomechanics symposium. San Francisco, California: American Rock Mechanics Association; 2015. ARMA-2015-430.
Ghazvinian E, Diederichs MS, Quey R. 3D random Voronoi grain-based models for simulation for brittle rock damage and fabric-guided micro-fracturing. Journal of Rock Mechanics and Geotechnical Engineering 2014;6(6):506–21.
Grau RH, Krog RB, Robertson SB. Maximizing the ventilation of large-opening mines. In: Proceedings of the 11th US/North American mine ventilation symposium. PA: University Park; 2006. p. 1–7.
Guo S, Qi S, Zou Y, Zheng B. Numerical studies on the failure process of heterogeneous brittle rocks or rock-like materials under uniaxial compression. Materials 2017;10(4):378.
Hajiabdolmajid V, Kaiser PK, Martin CD. Modelling brittle failure of rock. International Journal of Rock Mechanics and Mining Sciences 2002;39(6):731–41.
Hedley DGF, Grant F. Stope and pillar design for the Elliot Lake uranium mines. The Canadian Mining and Metallurgical Bulletin 1972;65:1165–86.
Hoek E, Carranza-Torres C, Corkum B. Hoek-Brown failure criterion—2002 edition. In: Proceedings of NARMS-TAC conference, Toronto, Canada; 2002. p. 267–73.
Hsu S, Nelson PP. Material spatial variability and slope stability for weak rock masses. Journal of Geotechnical and Geoenvironmental Engineering 2006;132(2):183–93.
Hudyma MR. Rib pillar design in open stope mining [MSc Thesis]. The University of British Columbia; 1988.
Iannacchione AT. Analysis of pillar design practices and techniques for US limestone mines. Transactions of the Institution of Mining & Metallurgy (Section A) 1999;108:A152–60.
Itasca FLAC. 3D version 5.0: theory and background. Minneapolis, Minnesota, USA: Itasca Consulting Group; 2016.

Jaeger JC, Cook NGW. Fundamentals of rock mechanics. 3rd ed. London: Chapman & Hall; 1979.
Jing L, Stephansson O. Fundamental of discrete element methods for rock engineering: theory and application. Amsterdam, Netherland: Elsevier; 2007.
Kaiser PK, Kim B, Bewich RP, Valley B. Rock mass strength at depth and implication for pillar design. Mining Technology 2011;120(3):170–9.
Kaiser PK, Kim B. Characterization of strength of intact brittle rock considering confinement-dependent failure processes. Rock Mechanics and Rock Engineering 2015;48(1):107–19.
Krauland N, Soder PE. Determining pillar strength from pillar failure observation. Engineering and Mining Journal 1987;188(8):34–40.
Lan H, Martin CD, Hu B. Effect of heterogeneity on brittle rock on micromechanical extensile behavior during compression testing. Journal of Geophysical Research: Solid Earth 2010;115(B1):14. https://doi.org/10.1029/2009JB006496.
Langford JC, Diederichs MS. Quantifying uncertainty in Hoek-Brown intact strength envelope. International Journal of Rock Mechanics and Mining Sciences 2015;74:91–102.
Lisjak A, Grasselli G. A review of discrete modeling techniques for fracturing processes in discontinuous rock masses. Journal of Rock Mechanics and Geotechnical Engineering 2014;6(4):301–14.
Mark C. Pillar design methods for longwall mining. U.S. Department of the Interior, Bureau of Mines; 1990. p. 53. IC 9247.
Mark C, Chase FE. Analysis of retreat mining pillar stability (ARMPS). In: Proceedings of new technology for ground control in retreat mining. U.S. Department of Health and Human Services, National Institute for Occupational Safety and Health (NIOSH); 1997. p. 17–34. IC 9446.
Martin CD, Chandler NA. The progressive fracture of Lac Du Bonnet granite. International Journal of Rock Mechanics and Mining Sciences & Geomechanics Abstracts 1994;31(6):643–59.
Martin CD. Seventeenth Canadian Geotechnical Colloquium: the effect of cohesion loss and stress path on brittle rock strength. Canadian Geotechnical Journal 1997;34(5):698–725.
Martin CD, Kaiser PK, McCreath DR. Hoek-Brown parameters for predicting the depth of brittle failure around tunnels. Canadian Geotechnical Journal 1999;36(1):136–51.
Martin CD, Maybee WG. The strength of hard rock pillar. International Journal of Rock Mechanics and Mining Sciences 2000;37(8):1239–46.
Mayer JM, Stead D. Exploration into the causes of uncertainty in UDEC grain boundary models. Computers and Geotechnics 2017;82:110–23.
Mortazavi A, Hassani FP, Shabani M. A numerical investigation of rock pillar failure mechanism in underground openings. Computers and Geotechnics 2009;36(5):619–97.
Munjiza A. The combined finite–discrete element method. John Wiley and Sons, Inc.; 2004.
Nicksiar M, Martin CD. Evaluation of methods for determining crack initiation in compression tests on low-porosity rocks. Rock Mechanics and Rock Engineering 2012;45(4):607–17.
Patton FD. Multiple modes of shear failure in rock. In: Proceedings of the 1st congress ISRM. Lisbon: ISRM; 1966. p. 509–13.
Pelli F, Kaiser PK, Morgenstrern NR. An interpretation of ground movements recorded during construction of the Donkin-Morien tunnel. Canadian Geotechnical Journal 1991;28(2):239–54.
Reinsalu E. Stochastic approach to room and pillar failure in oil shale mining. Proceedings of the Estonian Academy of Sciences 2000;6(3):207–16.
Renani HR, Martin CD. Modeling the progressive failure of hard rock. Tunnelling and Underground Space Technology 2018;74:71–81.
Ryder JA, Ozbay MU. A methodology for designing pillar layouts for shallow mining. In: International symposium on static and dynamic considerations in rock engineering. Swaziland: ISRM; 1990.
Schmertmann JH, Osterberg JO. An experimental study of the development of cohesion and friction with axial strain in saturated cohesive soils. Research conference on shear strength of cohesive soils. 1960. p. 643–94. Boulder, CO, USA.
Sinha S, Chugh YP. An evaluation of roof support plans at two coal mines in Illinois using numerical models. International Journal of Rock Mechanics and Mining Sciences 2016;82:1–9.
Sinha S, Walton G. Insight into hard rock pillar behavior from numerical simulation using a progressive S-shaped failure criterion. In: Proceedings of 51st US rock mechanics/geomechanics symposium. San Francisco, USA: American Rock Mechanics Association; 2017.
Sinha S, Walton G. A progressive S-shaped yield criterion and its application to the study of rock pillar behavior. International Journal of Rock Mechanics and Mining Sciences 2018;105:98–109.
Sjoberg J. Failure modes and pillar behavior in the Zinkgruvan mine. In: Proceedings of the 33rd U.S. rock mechanics symposium. American Rock Mechanics Association; 1992. p. 491–500.
Tang C. Numerical simulation of progressive rock failure and associated seismicity. International Journal of Rock Mechanics and Mining Sciences 1997;34(2):249–61.
Valley B, Kim B, Suorineni FT, Bahrani N, Bewick RP. Influence of confinement dependent failure processes on rock mass strength at depth. In: Qian Q, Zhou Y, editors. ISRM 12th international congress on rock mechanics. London: Springer; 2011. p. 855–60.
Vermeer PA, De Borst R. Non-associated plasticity for soils, concrete and rock. Heron 1984;29(3):1–64.
Wagner H. Determination of the complete load-deformation characteristics of coal pillars. In: Proceedings of the congress of the international society for rock mechanics. Denver, CO, USA: IRSM; 1974. p. 1067–81.
Wagner H. Pillar design in coal mines. Journal of the South African Institute of Mining & Metallurgy 1980;80(1):37–45.
Walton G. Improving continuum models for excavations in rock masses under high stress through an enhanced understanding of post-yield dilatancy [PhD Thesis]. Kingston, Canada: Queen's University; 2014.
Walton G, Diederichs MS, Punkkinen A. The influence of constitutive model selection on predicted stresses and yield in deep mine pillars — a case study at the Creighton mine, Sudbury, Canada. Geomechanics and Tunneling 2015;8(5):441–9.
Walton G, Diederichs MS. A new model for the dilation of brittle rocks based on laboratory compression test data with separate treatment of dilatancy mobilization and decay. Geotechnical and Geological Engineering 2015a;33(3):661–79.
Walton G, Diederichs MS. A mine shaft case study on the accurate prediction of yield and displacements in stressed ground using lab-derived material properties. Tunnelling and Underground Space Technology 2015b;49:98–113.
Walton G, Diederichs MS, Punkkinen A, Whitmore J. Back analysis of a pillar monitoring experiment at 2.4 km depth in the Sudbury Basin, Canada. International Journal of Rock Mechanics and Mining Sciences 2016;85:33–51.
Walton G, Hedayat A, Kim E, Labrie D. Post-yield strength and dilatancy evolution across the brittle-ductile transition in Indiana limestone. Rock Mechanics and Rock Engineering 2017;50(7):1691–710.
Wilson AH. The stability of underground workings in the soft rocks of coal measures. Geotechnical and Geological Engineering 1983;1(2):91–187.
Yan C, Zheng H, Sun G, Ge X. Combined finite-discrete element method for simulation of hydraulic fracturing. Rock Mechanics and Rock Engineering 2016;49(4):1389–410.
Zhao XG, Cai M. A mobilized dilation angle model for rocks. International Journal of Rock Mechanics and Mining Sciences 2010;47(3):368–84.
Zhao XG, Cai M, Cai M. Considerations of rock dilation on modeling failure and deformation of hard rocks—a case study of the mine-by test tunnel in Canada. Journal of Rock Mechanics and Geotechnical Engineering 2010;2(4):338–49.

Sankhaneel Sinha obtained his BE degree in Mining Engineering from Indian Institute of Engineering, Science and Technology, India in 2014 and his MS degree in Mining Engineering from Southern Illinois University Carbondale, United States, in 2016. He is currently pursuing his PhD in Colorado School of Mines, United States. His research interests include in situ instrumentation of coal/non-coal pillars and numerical simulation of mining ground control problems using continuum and dis-continuum approaches.